Electrochimica Acta 55 (2010) 8430–8438

Contents lists available at ScienceDirect

Electrochimica Acta

journal homepage: www.elsevier.com/locate/electacta

Advanced anticorrosive coatings prepared from electroactive polyimide–TiO_2 hybrid nanocomposite materials

Chang-Jian Weng[a], Jane-Yu Huang[a], Kuan-Yeh Huang[c], Yu-Sian Jhuo[a], Mei-Hui Tsai[b], Jui-Ming Yeh[a,*]

[a] Department of Chemistry and Center for Nanotechnology at CYCU, Chung Yuan Christian University, No. 200, Chung-Pei Road, Chung Li 32023, Taiwan, ROC
[b] Department of Chemical and Materials Engineering, Chin-Yi Institute of Technology, Taichung 41111, Taiwan, ROC
[c] Material and Chemical Research Laboratories, Industrial Technology Research Institute, Hsin-Chu 310, Taiwan, ROC

ARTICLE INFO

Article history:
Received 23 February 2010
Received in revised form 20 July 2010
Accepted 23 July 2010
Available online 30 July 2010

Keywords:
Nanocomposite
Titania
Polyimide
Corrosion
Electroactive

ABSTRACT

In this study, we present the first preparation and corrosion protection studies of a series of electroactive polyimide–TiO_2 (EPTs) hybrid nanocomposite materials containing conjugated segments of electroactive amino-capped aniline trimer (ATs) and TiO_2 nanoparticles of ~10 nm in diameter. Redox behavior of as-prepared EPTs hybrid materials was identified by electrochemical cyclic voltammetry (CV) studies. Higher concentration of TiO_2 component in as-prepare corresponding EPTs was found to reveal better corrosion protection effect on cold-rolled steel (CRS) electrode based on sequential electrochemical corrosion measurements in 5 wt.% NaCl electrolyte. Enhancement of corrosion protection of EPTs coatings on CRS electrode could be interpreted by following three possible reasons: (1) Electroactive polyimide (EPI) could act as a physical barrier coating. (2) The redox catalytic capabilities of ATs units existed in EPTs may induce the formation of passive metal oxide layers on CRS electrode. (3) The well-dispersed TiO_2 nanoparticles in EPTs matrix could act as effective hinder to enhance the oxygen barrier property of EPTs.

1. Introduction

Conducting polymers, such as polypyrrole, polythiophene, polyaniline, etc., consisting conjugated electronic structures have received considerable attention lately because of many promising technological applications [1–6]. Some specific conducting polymers such as polyaniline (PANI) and its derivatives were found to be applied as potentially advanced anticorrosion coatings due to its catalytic redox property resulted from conjugated chemical structures. For example, Wei et al. [7] evaluated the corrosion protection effect of PANI through performing a series of electrochemical measurements in saline condition. Some academic literatures reported that PANI coatings were found to reveal better anticorrosion properties on metallic substrate than several polymers [8–11]. DeBerry [12] claimed that PANI electrochemically deposited on stainless steel could provide a form of anodic protection. Mechanism for enhanced corrosion protection of conjugated PANI coatings had been suggested due to the formation of protective passivation oxide layer induced from the redox catalytic (i.e., electroactivity) capability of PANI [13–15].

Currently, aniline oligomer-derivating electroactive polymers had attracted considerable research attentions. For example, the preparation and electrochemical behavior of electroactive polyimide had been reported by Wang et al. [16,17] and Wei et al. [18]. Furthermore, the electrochemical behaviors of electroactive polyamide with amine-capped aniline pentamer prepared by oxidative coupling polymerization had also been demonstrated by Zhang and co-workers [17–21]. Lately, Yeh et al. reported the corrosion protection effect of organo-soluble electroactive polyimide containing amine-capped aniline trimer coated onto cold-rolled steel (CRS) electrode by performing series of electrochemical corrosion measurements in saline condition [22].

On the other hand, sol–gel deposited inorganic materials such as TiO_2/SiO_2 mixtures have been shown to work as protective coatings on stainless steel [23–27], however, annealing at high temperatures (800 °C) is required to obtain a well-defined crystalline structure. Such high temperature exposure can be problematic since it can modify the crystalline structure and the physical and/or mechanical properties of the steel. Titanium oxide films have also been prepared by vapour deposition techniques such as evaporation [28], sputtering [29,30], ion-assisted deposition [31], and low-pressure chemical vapour deposition [32]. However, uniform, large area thin films with precisely controlled thickness are difficult to achieve with these preparation techniques. In addition, vapour deposition entails a capital equipment cost that can be prohibitively high, especially for large area applications and there is considerable art associated with the design of the deposition systems and control of the operating parameters.

* Corresponding author. Tel.: +886 3 2653340; fax: +886 3 2653399.
E-mail address: juiming@cycu.edu.tw (J.-M. Yeh).

0013-4686/$ – see front matter © 2010 Elsevier Ltd. All rights reserved.
doi:10.1016/j.electacta.2010.07.063

Recently, potential advanced coatings prepared from organic–inorganic hybrid technology such as polymer–nanofiller hybrid materials had been reported [33–49]. In the studies of Yeh et al., the incorporation of well-dispersed clay platelets or nanosilica particles in polymer matrix was found to effectively enhance the corrosion protection of neat polymer coatings. It should be noted that the mechanism of enhanced corrosion protection of polymer/clay or polymer/silica nanocomposite coatings was resulted from the loading of effectively dispersed nanofiller, leading to a remarkably increased tortuosity of diffusion pathway of O_2 and H_2O molecules in the polymeric matrix. As titanium dioxide was commonly used as a pigment material for paints, it was thought worthwhile to use nano-particulate TiO_2 as a metal oxide additive in the composite which could give better dispersion of the formulation as well as barrier properties in the coatings [20].

However, practical applications of electroactive polyimide (EPI) hybrid materials containing nanoparticles (such as TiO_2 or SiO_2) have never been mentioned. Therefore, in this work, we present the first preparation of electroactive polyimide–TiO_2 (EPTs) hybrid nanocomposite materials and evaluate their corrosion protection effect on cold-rolled steel (CRS) electrode based on a series of electrochemical corrosion measurements in saline condition and barrier properties by gas permeability analysis (GPA).

2. Experimental

In this paper, we used two kinds of diamine to prepare non-electroactive polyimide and electroactive polyimide, respectively [50]. We used oxydianiline (ODA) as a diamine to synthesise the non-electroactive polyimide and N,N′-bis(4′-aminophenyl)-1,4-quinonenediimine (AT) as a diamine to synthesis the electroactive polyimide materials, because AT has conjugate segment in molecular structure.

2.1. Instrumentations and measurements

Aniline (Sigma–Aldrich) was distilled prior to use. 4,4′-Oxydianiline (ODA; Fluka, Buchs, Switzerland), 1,4-phenylenediamine (Sigma–Aldrich), N,N-dimethylacetamide (DMAc; Mallinckrodt/Baker, Paris, KY), 4,4′-(4,4′-isopropylidenediphenoxy)-bis(phthalic anhydride) (BSAA; Sigma–Aldrich, 97%) were used as received without further purification. Titanium (IV) n-butoxide (($Ti(OBu)_4$;Acros, 99%) and acetylacetone (ACAC; Fluka) were also used as received. All reagents were reagent grade unless otherwise stated.

Observation of the dispersion of silica particles was done using LV-SEM (S-3500N, Hitachi, Japan) with an EDS system (NORAN, Vantage) TEM images of the EPT nanocomposites were obtained with JEOL-200FX operated at an accelerating voltage of 120 kV. Electrochemical measurements of corrosion potential, polarization resistance, and corrosion current of coated cold-rolled steel (CRS) electrodes were obtained using VoltaLab 21 and VoltaLab 40 potentiostat/galvanostat with an electrochemical corrosion cell consisting of graphite rod counter electrode, SCE reference electrode and working electrode. Lastly, gas permeability (O_2 permeation) experiments were achieved using GTR-31 analyzer (Yangimoto Co., Kyoto, Japan).

2.2. Synthesis of N,N′-bis(4′-aminophenyl)-1,4-quinonenediimine (ATs)

A typical procedure was recently established by Wei et al. for the synthesis of the aniline trimer (ATs) and accordingly, ATs could be easily synthesized by oxidative coupling of 1,4-phenylenediamine and two equivalent amounts of aniline with ammonium persulfate as oxidant [18].

2.3. Preparation of non-electroactive polyimide (NEPI) films

A typical procedure to prepare the non-electroactive polyimide was given as follows: BSAA (0.26 g, 0.5 mmol) was added to 4.0 g of DMAc at room temperature, with continuous stirring for 30 min. A separate solution containing ODA (0.1 g, 0.5 mmol) in another 4 g of DMAc was prepared under mechanical stirring. After stirring for 30 min, both were subsequently mixed. The as-prepared mixture was then stirred for an additional 2 h at room temperature under nitrogen. It was subsequently poured onto the supporting substrate to form the electroactive polyimide and then dried under vacuum at 60 °C for 3 h, 100 °C for 1 h, 200 °C for 1 h and 250 °C for 4 h, sequentially, to give NEPI material.

2.4. Preparation of electroactive polyimide (EPI) films

A typical procedure to prepare the non-electroactive polyimide was given as follows: BSAA (0.26 g, 0.5 mmol) was added to 4.0 g of DMAc at room temperature, with continuous stirring, for 30 min. A separate solution containing ATs (0.145 g, 0.5 mmol) in another 4 g of DMAc was prepared under mechanical stirring. After stirring for 30 min, both were subsequently mixed. The as-prepared mixture was then stirred for an additional 2 h at room temperature under nitrogen. It was subsequently poured onto the supporting substrate to form the electroactive polyimide and then dried under vacuum at 60 °C for 3 h, 100 °C for 1 h, 200 °C for 1 h and 250 °C for 4 h, sequentially, to give EPI material [22].

2.5. Preparation of electroactive polyimide–TiO_2 (EPTs) hybrid films

EPTs were prepared using N,N′-bis(4′-amino-phenyl)-l,4-quinonenediimine (AT), 0.145 g is added into a flask and dissolved in 4 g of DMAc with magnetic stirring for 30 min. Subsequently, the calculated amount of $Ti(OBu)_4$ and ACAC was completely mixed and added dropwise into the previous as-prepared solution under vigorous stirring to avoid local inhomogeneity. The blending mixture proceeded with continuous stirring for another 1 h at room temperature. For the preparation of poly(amic acid) (PAA) solution, 0.26 g of 4,4′-(4,4′-isopropylidenediphenoxy)bis(phthalic anhydride) (BSAA) was added and reacted at room temperature under nitrogen. After 2 h, the as-prepared PAA solution was cast onto glass substrate, followed by programmed drying at 60 °C for 3 h, 100 °C for 1 h, 200 °C for 1 h and 250 °C for 4 h, sequentially, to give series of EPTs hybrid nanocomposite materials. The synthesis procedure of EPTs is depicted in Scheme 1.

2.6. Electrochemical cyclic voltammetric (CV) studies on the electroactivity of as-prepared EPI and EPTs

Electroactive experiments were performed on VoltaLab 40 (PGZ 301) analytical voltammeter using a conventional three-electrode system. All the CV measurements were performed at a double-wall jacketed cell, covered with a glass plate, through which water was circulated from a YEONG SHIH B-20 thermostat to maintain a constant operational temperature of 25 ± 0.5 °C. The as-prepared polyimide film-coated electrode was prepared by casting the polymer solution in DMAc (0.25 M) on top of the working electrode and then drying it in air. The platinum foil (applied surface area = 1 cm^2) was acted as a working electrode, a platinum wire and saturated calomel electrode (SCE) were used as counter and reference electrode, respectively. The working electrode coated polyimide thin film was then scanned by potential cyclic between 0 and 0.9 V

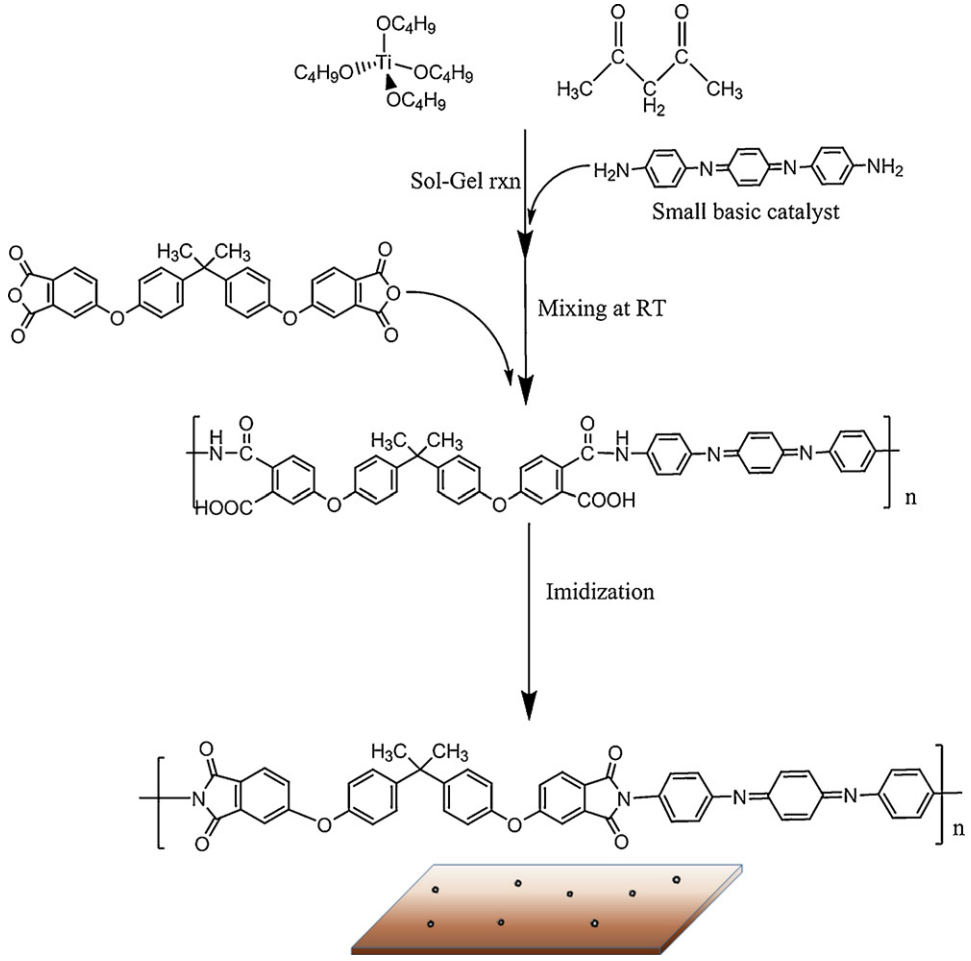

Scheme 1. Schematic representation of the synthesis of electroactive polyimide–TiO_2.

with a scan rate of 50 mV s^{-1} in 1 M H_2SO_4. The electrochemical CV measurements of all samples were repeated at least three times to ensure consistence.

2.7. Electrochemical corrosion evaluations of EPI and EPTs

To measure the electrochemical corrosion performance of sample-coated CRS electrodes, a series of EPTs were first cast dropwisely onto the CRS coupons (1.0 cm × 1.0 cm), followed by drying in air at 250 °C for 4 h for allowing the evaporation of solvent molecules to give an uniform and dense coatings of about 20 ± 2 μm in thickness, measured by digimatic micrometer (Mitutoyo, Japan). The coated and uncoated coupons were then mounted to the working electrode so that only the coated side of the coupon was in direct contact with the electrolyte. The edges of the coupons were sealed with super fast epoxy cement (SPAR®). All the electrochemical corrosion measurements and impedance spectroscopy were performed on a VoltaLab 21 (PGP 201) and repeated at least three times to ensure a reproducible result. All the electrochemical corrosion measurements were also performed at a double-wall jacketed cell, covered with a glass plate, through which water was circulated from a YEONG SHIH B-20 thermostat to maintain a constant operational temperature of 25 ± 0.5 °C. As electrolyte, aqueous solutions of NaCl (5 wt.%) were used. Open circuit potential (OCP) at the equilibrium state of the system was recorded as the corrosion potential (E_{corr} in mV vs. SCE). Polarization resistance (R_p in Ω/cm^2) was measured by sweeping the applied potential from 20 mV below to 20 mV above the E_{corr} at a scan rate of 10 mV/min and recording the corresponding current change. R_p value was obtained from the slope of the potential–current plot. The Tafel plots were obtained by scanning the potential from 250 mV below to 250 mV above the E_{corr} at a scan rate of 10 mV/min. Corrosion current (I_{corr}) was determined through superimposing a straight line along the linear portion of the cathodic or anodic curve and extrapolating it through E_{corr}. The corrosion rate (R_{corr}, in millimer per year) was calculated from the following equation:

$$R_{corr}\,(\mathrm{mm/year}) = \frac{[I_{corr}\,(\mathrm{A/cm^2}) \cdot M(\mathrm{g})]}{D\,(\mathrm{g/cm^2}) \cdot V} \times 3270$$

where I is the current (A/cm^2), M is the molecular weight, V is valence, 3270 is constant and D is the density (g/cm^3). VoltaLab 40 (PGZ 301) potentiostat/galvanostat was employed to perform the a.c. impedance spectroscopy measurements. Impedance measurements were carried out in the frequency range of 100 K–100 mHz. The working electrode was first maintained in the test environment for 30 min before the impedance run. This step served to put the electrode in a reproducible initial state and to make sure that no blistering occurred during the conditioning period. All experiments were operated at room temperature. All raw data were repeated at least three times to ensure reproducibility and statistical significance.

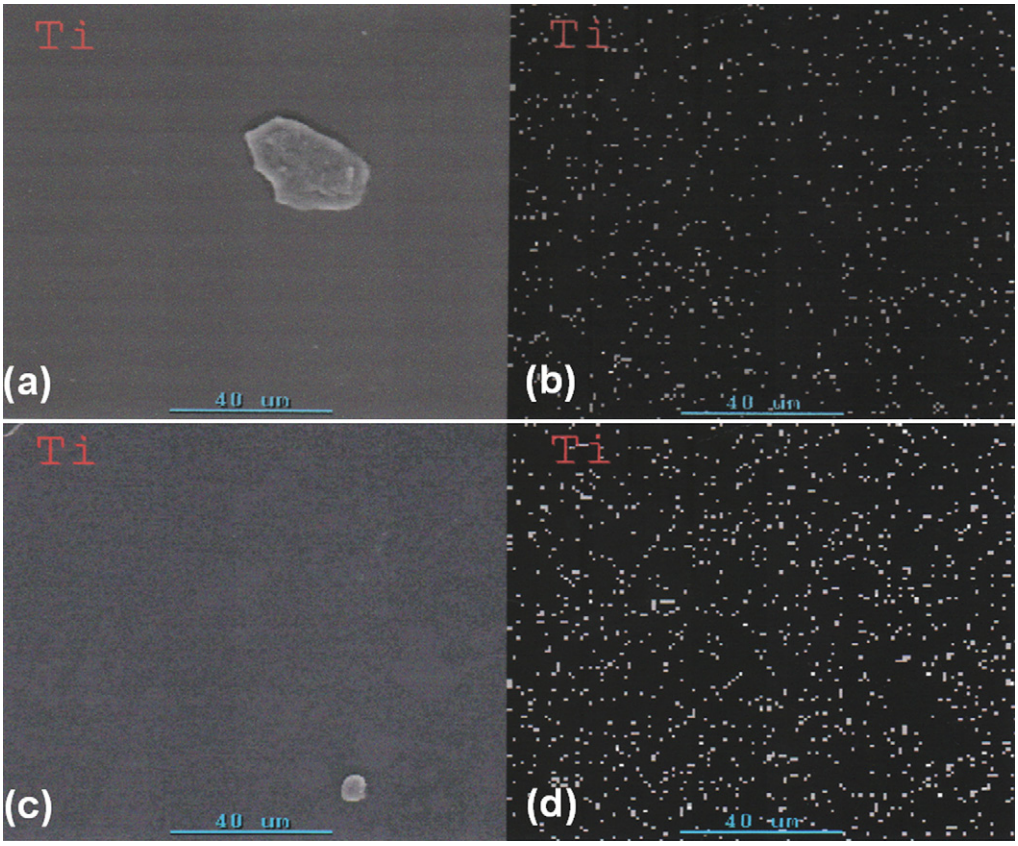

Fig. 1. Series of SEM mapping images of EPTs containing 5 wt.% and 10 wt.% TiO_2: (a) as-made EPT05; (b) Ti-mapping of EPT05; (c) as-made EPT10; (d) Ti-mapping of EPT10.

3. Results and discussion

3.1. Synthesis and characterization

The TiO_2 nanoparticles distributions in the EPI polymer matrix were also studied using an SEM mapping technique. A series of SEM elemental mapping images (Fig. 1) of the as-synthesized samples show that, from a macroscopic view, the TiO_2 particles were evenly distributed throughout the composite samples. More densified TiO_2 distributions were observed for higher TiO_2 content samples (Fig 1(d)). Thus, these morphological studies demonstrated that TiO_2 nanoparticles had been successfully prepared and dispersed within the EPI matrix.

Transmission electron microscopy (TEM) was used to investigate three-dimensional morphological images of as-prepared hybrid matrices. Fig. 2(a) and (b) demonstrates that EPTs hybrid material incorporated with 10 wt.% TiO_2 concentration exhibited a good dispersion of TiO_2 with ~10 nm in diameter existed in hybrid matrix. Typically, the bright region in TEM photograph represented the domain of neat EPI matrix and the dark-color spots correspond to dispersed phase of TiO_2 nanoparticles, respectively. It was found that the average particle size of TiO_2 was ca. at approximated size of 10 ± 3 nm in diameter.

3.2. Thermal properties of EPI and EPTs coatings

The decomposition temperatures (T_d) at onset point are listed in Table 1. The result indicates that the decomposition temperature of onset point is all above 490 °C for EPTs with TiO_2 content lower than 10 wt.% and decreased with the increase of TiO_2 content. According to the previous studies, the decrease in thermal stability could be attributed to the metallic compounds, which can oxidatively degrade polyimide films (about 490 °C) [51–54]. Although the introduction of TiO_2 causes a decrease in thermal stability, but the char yield after 800 °C decomposition is increased with the increase of TiO_2 content because metal oxide TiO_2 cannot decompose in high temperature. All the hybrid films still possess pretty good thermal stability.

3.3. Electroactivity of EPI and EPTs coatings

Cyclic voltammetry (CV) has been widely used to characterize the electrochemical properties of electroactive polymers. In this paper, the polymers were characterized by CV using a three-electrode electrochemical cell. As shown in Fig. 3, the electrochemical cyclic voltammetric studies indicated that all EPTs (e.g., EPT05 and EPT10), in the form of coating, showed single oxidation peak, which was similar to EPI [36]. Furthermore, the as-prepared EPTs with different feeding ratios of TiO_2 nanoparticles remain exhibited obviously electroactivity properties. For example, the EPT10 revealed oxidation current (I_{ox}) of 33.57 μA/cm^2 and reduction current (I_{red}) of 55.79 μA/cm^2, respectively. This was smaller than that of EPI (I_{ox} = 38.82 μA/cm^2, I_{red} = 68.28 μA/cm^2). However, NEPI showed null zero redox current. This implied that the incorporation of ATs into the polyimide may introduce the electroactivity into as-prepared polyimide. While the incorporation of TiO_2 into EPI matrix, which may maintain the EPTs films higher electroactivity. We therefore envisioned that the EPTs in the form of coating may reveal an effectively enhanced corrosion protection effect that was a result of synergistic effect of passive metal oxide layer and TiO_2 nanoparticles act as effective hinder to enhance the oxygen barrier property, based on a series of electrochemical standard corrosion measurements (e.g., potentiodynamic and electrochemical impedance measurements) and gas barrier measurement as discussed in the following sections.

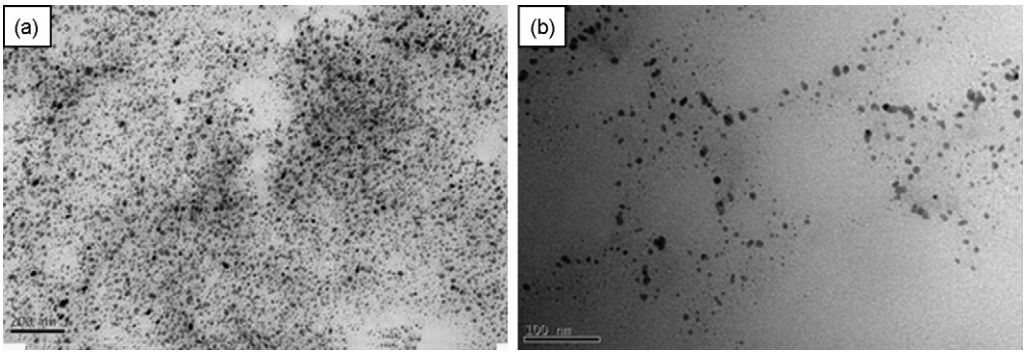

Fig. 2. TEM images of EPT10 (a) 20K× (b) 50K×.

Table 1
Feed composition ratio, electrochemical corrosion measurements and thermal properties of the prepared materials.

Sample code	Feed composition (g)				Electrochemical corrosion measurements						Thermal properties[a]	
	ODA	ATs	BSAA	$Ti(OBu)_4$	E_{corr} (mV)	R_p (KΩ cm^2)	I_{corr} μA/cm^2	R_{corr} (mm/year)	Thickness (μm)	P_{EF} (%)	T_d[b] (°C)	Char yield[c] (%)
Bare[d]	–	–	–	–	−976.9	0.011	5.275	6.2×10^{-2}	–	–	–	–
NEPI	0.1	–	0.26	–	−647.8	0.074	0.700	8.2×10^{-3}	20	5.98	–	–
EPI	–	0.145	0.26	–	−469.5	0.112	0.598	7.0×10^{-3}	20	9.56	527.52	0.81
EPT05	–	0.145	0.26	0.203	−330.4	0.271	0.333	3.9×10^{-3}	22	24.56	509.17	2.12
EPT10	–	0.145	0.26	0.405	−179.0	0.439	0.164	1.9×10^{-3}	21	40.37	498.13	3.37

[a] As measured by thermogravimetric analysis (TGA) at 10 °C/min in air condition.
[b] Temperature at onset point.
[c] Char yield at 800 °C.
[d] Pristine CRS used for test.

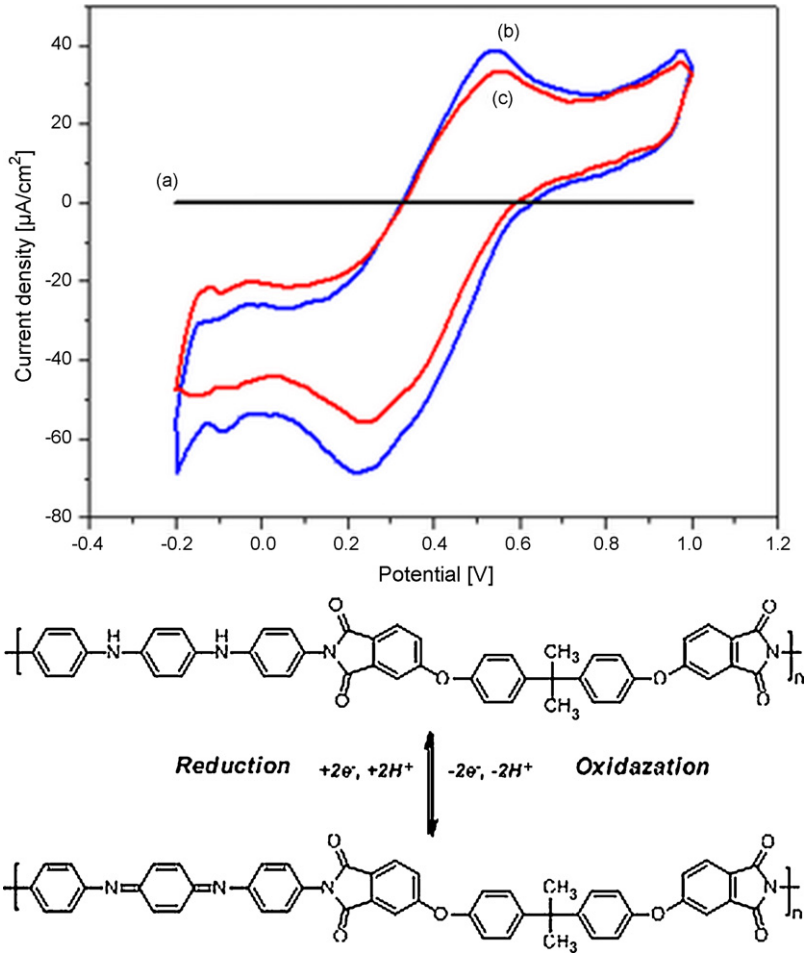

Fig. 3. Cyclic voltammetry of the polyimide shown as (a) NEPI, (b) EPI and (c) EPT10 above were measured in aqueous H_2SO_4 (1.0 M) with scan rate of 50 mV/s. The proposed oxidation mechanism is shown.

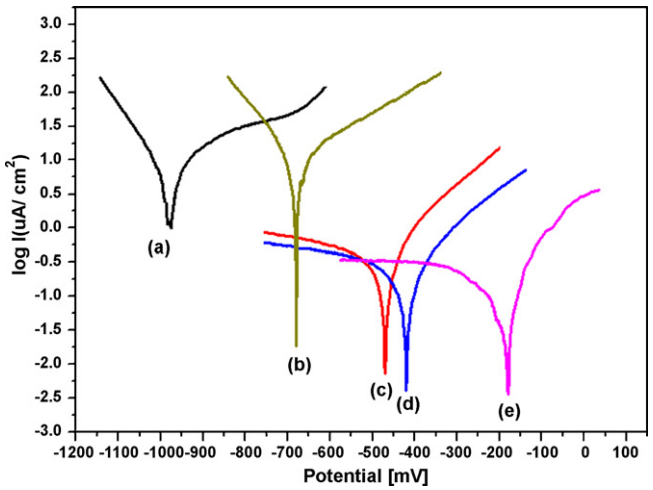

Fig. 4. Tafel plots for (a) NEPI, (b) EPI and (c) EPT05 (d) EPT10 measured in 5 wt.% aqueous NaCl solution.

3.4. Potentiodynamic measurements

In this section, corrosion protection of sample-coated CRS coupons can be observed from the values of corrosion potential (E_{corr}), polarization resistance (R_p), corrosion current (I_{corr}), and corrosion rate (R_{corr}), as listed in Table 1.

The polarization resistances, R_p, were evaluated from the Tafel plots, according to the Stearn–Geary equation [55],

$$R_p = \frac{b_a b_c}{2.303(b_a + b_c) I_{corr}}$$

Here, I_{corr} is the corrosion current determined by an intersection of the linear portions of the anodic and cathodic curves, and b_a and b_c are anodic and cathodic Tafel slopes ($\Delta E/\Delta \log I$), respectively.

The protection efficiency (P_{EF}%) values were estimated using the following equation [56]:

$$P_{EF}\% = \frac{R_P{}^{-1}(\text{uncoated}) - R_P{}^{-1}(\text{coated})}{R_P{}^{-1}(\text{coated})} \times 100$$

The CRS coupon coated with EPI shows a higher E_{corr} value than the NEPI-coated CRS, which is consistent with previous observations [22]. It is worth to note that EPI with AT displays better corrosion protection performance on CRS electrode than NEPI that without ATs. However, it exhibits a lower E_{corr} value than the specimen coated with EPTs materials. For example, the EPT10-coated CRS has a high corrosion potential of ca. −179 mV at 30 min. Even after 5 h measurement, the potential remained at ca. −182 mV. Such a E_{corr} value implies that the EPT10-coated CRS is more noble toward the electrochemical corrosion compared to the EPI. The EPT10-coated CRS shows a polarization resistance (R_p) value of 0.439 kΩ cm^2 in 5 wt.% NaCl, which is about 1 order of magnitude greater than the uncoated CRS. The Tafel plots for (a) uncoated, (b) NEPI-coated, (c) EPI-coated, (d) EPT05-coated, and (e) EPT10-coated CRS are shown in Fig. 4. For example, the corrosion current (I_{corr}) of EPT10-coated CRS is ca. 0.164 μA/cm^2, which is correspondent to a corrosion rate (R_{corr}) of ca. 1.9×10^{-3} mm/year (Table 1). Electrochemical corrosion current and corrosion potential of EPTs materials as coatings on CRS were found to decrease gradually with further increase in TiO_2 loading. Enhanced corrosion protection effect of EPTs nanocomposite materials compared to EPI might be resulted from dispersing TiO_2 nanoparticles in EPI matrix to increase the tortuosity of diffusion pathway of oxygen gas. This is further evidenced by the studies of the O_2 gas barrier effect as discussed in the following section.

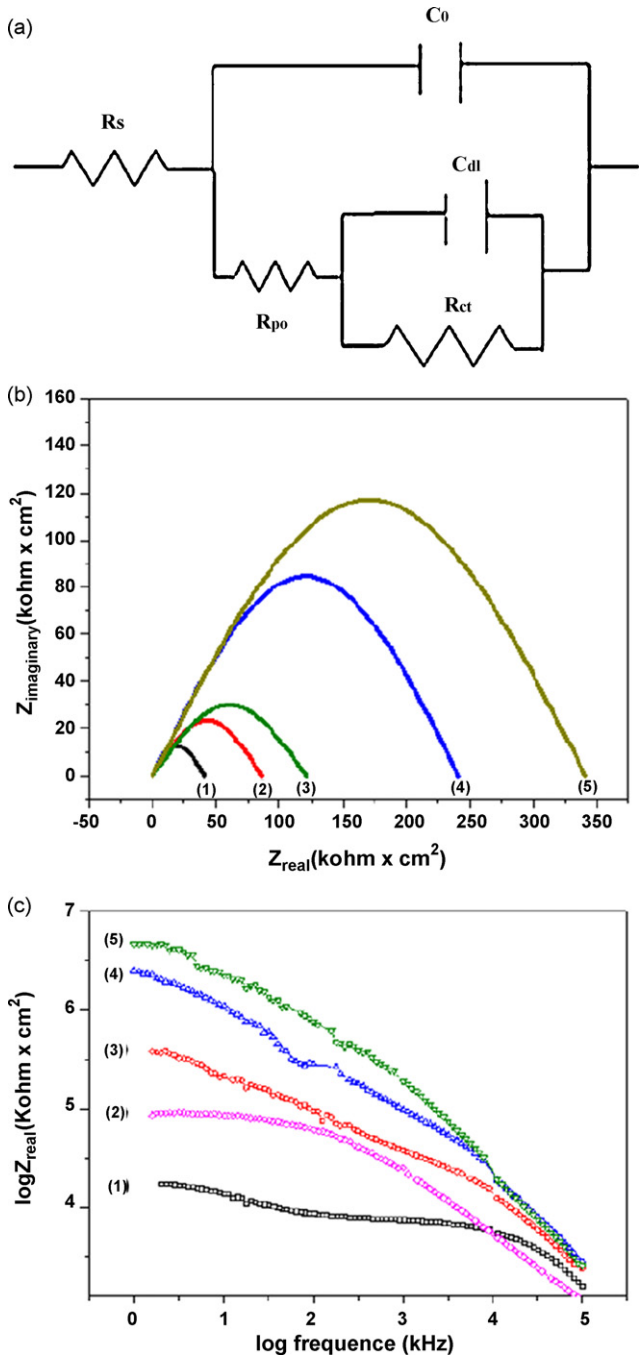

Fig. 5. (a) Analogue circuit, (b) Nyquist plots for (1) neat CRS, (2) NEPI, (3) EPI, (4) EPT05 and (5) EPT10-coated CRS electrode, measured in 5 wt.% aqueous NaCl solution. (c) Bode plots for (1) neat CRS, (2) NEPI, (3) EPI, (4) EPT05 and (5) EPT10-coated CRS electrode, measured in 5 wt.% aqueous NaCl solution.

3.5. Electrochemical impedance spectroscopy

Electrochemical impedance spectroscopy (EIS) was an alternative tool to evaluate the activity difference between surface of CRS electrode after NEPI, EPI and EPTs treatment. Impedance is totally complex resistance when a current flows through a circuit made of capacitors, resistors, or insulators, or any combination of these [56]. EIS measurement results in currents over a wide range in frequency. For the EPTs, an analogue circuit (called a Randles circuit), as represented in upper part of Fig. 5(a) could be used, in which together with the above traditional components. It is known that R_s is the solution resistance, C_c is the coating capacitance, R_{po} is the coating

pore resistance, while R_{ct} and C_{dl}, respectively, stand for the charge transfer resistance and the double layer capacitance which reflect states of the electrochemical reactions under the coating. For intact coatings, the coating resistance R_{po} is much higher compared with the electrochemical reaction parameters [57]. Supposing the solution resistance R_s is negligible, during the early period of immersion the equivalent circuit may be approximately expressed as a parallel connection of R_{po} and C_c, the impedance of which has following form [58,59]:

$$Z = \frac{R_{po}}{1 + (\omega C_c R_{po})^2} - \frac{j(\omega C_c R_{po}{}^2)}{1 + (\omega C_c R_{po})^2}$$

The high-frequency intercept is equal to the solution resistance, and the low-frequency intercept is equal to the sum of the solution and charge transfer resistances [60]. The higher the semicircle diameter (charge transfer resistance) the lower the corrosion rate [61,62]. The corrosion protection studies of these samples with 20 ± 2 μm in coating thickness immersed in 5 wt.% aqueous NaCl electrolyte for 30 min was followed by EIS. First of all, we found that the charge transfer resistance of samples as determined by the intersection of the low-frequency end of the semicircle arc with the real axis was 41.20, 86.31, 121.20, 241.79 and 340.90 kΩ cm^2, respectively (Fig. 5(b)). This result clearly demonstrated that the sample, with the highest content of TiO_2, had the greatest corrosion protection performance. It should be further noted that EPTs exhibited a higher charge transfer resistance (i.e., EPT10, 340.90 kΩ cm^2). According to Fig. 5(b) (curve (b)), the NEPI exhibits a charge transfer resistance of 41.20 kΩ cm^2. Furthermore, EIS Bode plots (impedance vs. frequency) of as-prepared EPTs are shown in Fig. 5(c). The increase of impedance value at high content of TiO_2 in the monitoring frequency region from low to high-frequency could be interpreted due to redox catalytic property of EPTs resulted from the TiO_2. Again, the EPTs coating, exhibited a higher charge resistance than that of NEPI and EPI, in the entire monitoring frequency range base on the studies of EIS Bode plots. Mechanism of enhanced corrosion protection of EPTs coatings was found to be associated with the formation of passivation protective metal oxide layers, inducing from the redox catalytic properties of ATs units existed in as-prepared EPTs coatings, as shown in Scheme 2(a). Mechanism of corrosion protection for the as-prepared EPTs was similar to that of PANI coatings reported in the previous literatures [13–15].

3.6. Observations and investigation on the CRS surface

In the present work, the as-prepared sample coatings were then removed by razor knife. Visual observation of the passivation oxide layers exhibited the deposition of grayish oxide layer form over the CRS surface [8] under the EPTs coating on CRS electrode. SEM image

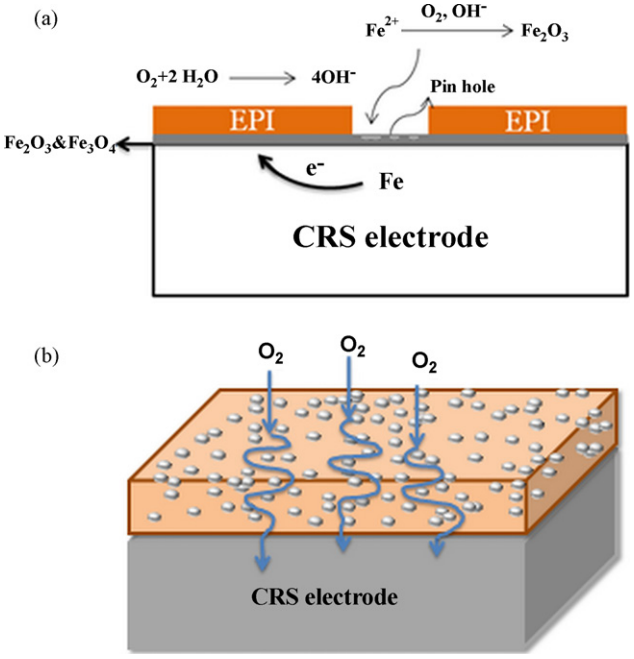

Scheme 2. Schematic diagrams of (a) mechanism of CRS passivation by EPT coatings and (b) diffusion pathway of oxygen gas in the EPT.

studies revealed that the oxide layers were formed at the interface of EPTs (i.e., EPT10) coating and the CRS surface (Fig. 6(b)) but we could not observe the same image from pure CRS surface (Fig. 6(a)).

3.7. Molecular barrier properties

The presence of filler, inorganic or organic, in the polymer matrix usually constitutes a solid barrier in the path of the gas molecules passing through the polymer. A more tortuous path is thus forced upon the gas molecules passing through the polymeric matrix, retarding the progress of the phenomenon. The more tortuous the path the longer it takes for the gas molecules to pass through the material, resulting in a macroscopically observed reduced permeability. The higher the filler–matrix interfacial area and aspect ratio of the filler, the more tortuous the path, hence the greater the decrease in permeability. This is the reason why nanocomposites are vigorously examined for their permeability rates' enhancements, due to their high interfacial area, and mostly in polymer/layered silicate nanocomposites, due to the high aspect ratio of the filler [63]. Although spherical TiO_2 nanoparticles are not considered the most effective barrier, as in the case of sheet-like layered silicates, where due to their high length-to-width ratio the

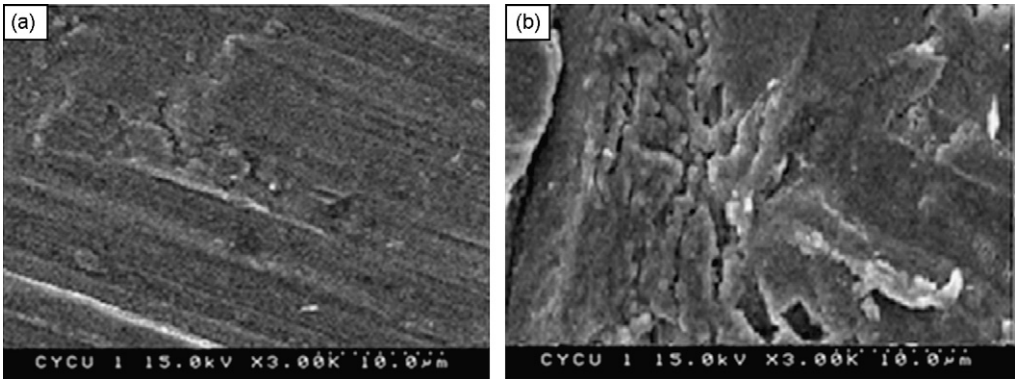

Fig. 6. SEM image for (a) polished CRS metal and the surface of the (b) EPT10 coating and the CRS metal.

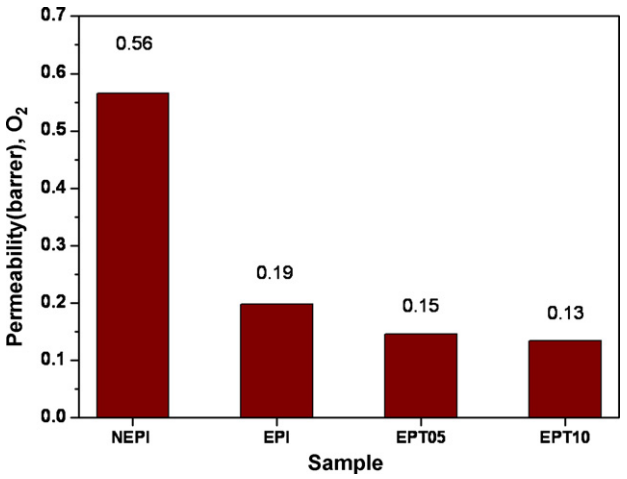

Fig. 7. Permeability of O_2 as a function of the TiO_2 content in the EPTs nanocomposite materials.

path length of the gas is maximized, nonetheless such nanoparticles should also significantly reduce gas diffusion through the material. In this study, the membranes of EPTs materials and EPI used for the molecular barrier measurements were prepared to have a film thickness of approximately 60 μm. In comparison with NEPI and EPI, the EPTs membranes prepared by both approaches exhibited lower O_2 permeability, as shown in Fig. 7.

For instance, the O_2 permeability of NEPI, EPI, EPT05 and EPT10 was ca. 0.56 barrer, 0.19 barrer, 0.15 barrer and 0.13 barrer, respectively. Compared with NEPI and EPI membranes, the O_2 permeability of NEPI is higher than EPI. The possible reason is that the dense packed structure of EPI membrane is formed by the intramolecular interactions such as π–π stacking between aromatic rings of ATs segment [64]. However, compared to that of EPI, the EPTs nanocomposite materials at low TiO_2 loading (e.g., EPT05) show about 21% reduction of O_2 permeability. This result could be associated with EPTs having a better dispersion of TiO_2 nanoparticles in the EPI matrix, which led to a remarkably increased tortuosity of the diffusion pathway of oxygen, as shown in Scheme 2(b). It was worth noticed that a further increase of TiO_2 loading results in a slightly further enhanced molecular barrier property of EPTs nanocomposite materials.

4. Conclusion

In this study, we present the first preparation and corrosion protection studies of a series of electroactive polyimide–TiO_2 (EPTs) hybrid nanocomposite materials containing conjugated segments of electroactive amino-capped aniline trimer (ATs) and TiO_2 nanoparticles of ~10 nm in diameter. Electroactivity of as-prepared EPTs hybrid materials was identified by the cyclic voltammetry (CV) studies. It should be noted that the EPTs having different content of TiO_2 still exhibited a redox current as compared to that of EPI. The as-prepared EPTs with higher content of TiO_2 exhibited obviously enhanced corrosion protection efficiency than NEPI on CRS electrodes, EPI on CRS electrodes and bare CRS was investigated by performing sequential electrochemical corrosion measurements in saline condition

The significant enhancement of corrosion protection on CRS electrodes might probably be attributed to the redox catalytic property of electroactive aniline trimer (ATs) in the formation of passive layer of metal oxide and the barrier affection of well-dispersed nanoparticles (TiO_2) existed in the polymer matrix. The ATs and TiO_2 content in the EPT hybrid materials act as a redox catalyst and barrier to increase the corrosion protecting ability, respectively. These EPTs show the excellent corrosion inhibition and promise anticorrosion materials in many applied fields.

Acknowledgments

The financial support of this research provided by the Ministry of Education, Taiwan, ROC, NSC-98-2113-M-033-001-MY3 and Department of Chemistry at CYCU, CYCU-98-CR-CH is gratefully acknowledged.

References

[1] S. Dogan, U. Akbulcin, S. Suzer, L. Toppare, Synth. Met. 60 (1993) 27.
[2] T. Kabayashi, H. Yoneyama, H. Tamura, J. Electroanal. Chem. 161 (1984) 419.
[3] E.W. Paul, A.J. Ricco, M.S. Wrighton, J. Phys. Chem. 89 (1985) 1441.
[4] Y. Cao, G.M. Treacy, P. Smith, A. Heeger, J. Appl. Phys. Lett. 60 (1992) 2711.
[5] V. Parkhutik, J. Martinez-Duart, C.R. Diaz, E.S. Matveeva, J. Electrochem. Soc. 140 (1993) L94.
[6] E. Matveeva, V. Parkhutic, C.R. Diaz, J. Martinez-Duart, J. Lumin. 57 (1993) 175.
[7] Y. Wei, J. Wang, X. Jia, J.M. Yeh, P. Spellane, Polymer 36 (1995) 4535.
[8] T.P. McAndrew, S.A. Miller, A.G. Gilicinski, L.M. Robeson, Mater. Sci. Eng. Polym. 74 (1996) 204.
[9] B. Wessling, J. Posdorfer, Electrochim. Acta 44 (1999) 2139.
[10] P.J. Kinlen, D.C. Silverman, C.R. Jeffreys, Synth. Met. 85 (1997) 1327.
[11] J.L. Camalet, J.C. Lacroix, S. Aeiyach, K. Chaneching, P.C. Lacaze, Synth. Met. 93 (1998) 133.
[12] D.W. DeBerry, J. Electrochem. Soc. 132 (1985) 1022.
[13] A. Talo, P. Passiniemi, O. Forsen, S. Ylasaari, Synth. Met. 85 (1997) 1333.
[14] G.M. Spinks, A.J. Dominis, G.G. Wallace, D.E. Tallman, J. Solid State Electrochem. 6 (2002) 85.
[15] P. Li, T.C. Tan, J.Y. Lee, Synth. Met. 88 (1997) 237.
[16] Z.Y. Wang, C. Yang, J.P. Gao, J. Lin, X.S. Meng, Y. Wei, S. Li, Macromolecules 31 (1998) 2702.
[17] W. Lu, X.S. Meng, Z.Y. Wang, J. Polym. Sci. A: Polym. Chem. 37 (1999) 4295.
[18] D. Chao, L. Cui, X. Lu, H. Mao, W.J. Zhang, Y. Wei, Eur. Polym. J. 43 (2007) 2641.
[19] D. Chao, X. Lu, J. Chen, X. Zhao, L. Wang, W.J. Zhang, Y. Wei, J. Polym. Sci. A: Polym. Chem. 44 (2006) 477.
[20] D. Chao, X. Ma, X. Lu, L. Cui, H. Mao, W.J. Zhang, Y. Wei, Macromol. Chem. Phys. 208 (2007) 658.
[21] D. Chao, X. Ma, X. Lu, L. Cui, H. Mao, W.J. Zhang, Y. Wei, J. Appl. Polym. Sci. 104 (2007) 1603.
[22] K.Y. Huang, Y.S. Jhuo, P.S. Wu, C.H. Lin, Y.H. Yu, J.M. Yeh, Eur. Polym. J. 45 (2009) 485.
[23] L. Bamoulid, M.T. Maurette, D. De Caro, A. Guenbour, A. Ben Bachir, L. Aries, S. El Hajjaji, F. Benoit-Marquie, F. Ansart, Surf. Coat. Technol. 202 (2008) 5020.
[24] D.Y. Shin, K.N. Kim, S.M. Han, Mater. Sci. Forum 486 (2005) 5.
[25] G.X. Shen, Y.C. Chen, C.J. Lin, Thin Solid Films 489 (2005) 130.
[26] M. Atik, P. de Lima Neto, M.A. Aegerter, L.A. Avaca, J. Appl. Electrochem. 25 (1995) 142.
[27] M. Atik, J. Zarzycki, J. Mater. Sci. Lett. 13 (1994) 1301.
[28] L.I. Maissel, R. Glang, Handbook of Thin Film Technology, first ed., McGraw-Hill, New York, USA, 1970.
[29] A.A. Soliman, H.J.J. Seguin, Solid Energy Mater. 5 (1981) 95.
[30] C. Fonseca, F. Vaz, M.A. Barbosa, Corros. Sci. 46 (2004) 3005.
[31] P.J. Martin, Vacuum 36 (1986) 585.
[32] J.P. Lu, J. Wang, R. Raj, Thin Solid Films 204 (1991) L13.
[33] J.M. Yeh, S.J. Liou, C.Y. Lin, C.Y. Cheng, Y.W. Chang, K.R. Lee, Chem. Mater. 14 (2002) 154.
[34] J.M. Yeh, S.J. Liou, M.C. Lai, Y.W. Chang, C.Y. Huang, C.P. Chen, J.H. Jaw, T.Y. Tsai, Y.H. Yu, J. Appl. Polym. Sci. 94 (2004) 1936.
[35] J.M. Yeh, S.J. Liou, C.G. Lin, Y.P. Chang, Y.H. Yu, C.F. Cheng, J. Appl. Polym. Sci. 92 (2004) 1970.
[36] J.M. Yeh, C.L. Chen, Y.C. Chen, C.Y. Ma, H.Y. Huang, Y.H. Yu, J. Appl. Polym. Sci. 92 (2004) 631.
[37] J.M. Yeh, H.Y. Huang, C.L. Chen, W.F. Su, Y.H. Yu, Surf. Coat. Technol. 200 (2006) 2753.
[38] J.M. Yeh, C.L. Chen, T.H. Kuo, W.F. Su, H.Y. Huang, D.J. Liaw, H.Y. Lu, C.F. Liu, Y.H. Yu, J. Appl. Polym. Sci. 92 (2004) 1072.
[39] Y.H. Yu, J.M. Yeh, S.J. Liou, C.L. Chen, D.J. Liaw, H.Y. Lu, J. Appl. Polym. Sci. 92 (2004) 3573.
[40] J.M. Yeh, C.F. Hsieh, J.H. Jaw, T.H. Kuo, H.Y. Huang, C.L. Lin, M.Y. Hsu, J. Appl. Polym. Sci. 95 (2005) 1082.
[41] Y.H. Yu, J.M. Yeh, S.J. Liou, Y.P. Chang, Acta Mater. 52 (2004) 475.
[42] J.M. Yeh, S.J. Liou, C.Y. Lai, P.C. Wu, T.Y. Tsai, Chem. Mater. 13 (2001) 1131.
[43] J.M. Yeh, C.L. Chen, Y.C. Chen, C.Y. Ma, K.R. Lee, Y. Wei, S. Li, Polymer 43 (2002) 2729.
[44] J.M. Yeh, C.P. Chin, J. Appl. Polym. Sci. 88 (2003) 1072.
[45] K.C. Chang, M.C. Lai, C.W. Peng, Y.T. Chen, J.M. Yeh, C.L. Lin, J.C. Yang, Electrochim. Acta 51 (2006) 5645.
[46] Y.H. Yu, C.C. Jen, H.Y. Huang, P.C. Wu, C.C. Huang, J.M. Yeh, J. Appl. Polym. Sci. 91 (2004) 3438.
[47] J.M. Yeh, C.P. Chin, S. Chang, J. Appl. Polym. Sci. 88 (2003) 3264.

[48] J. Park, J.W. Lee, D.W. Kim, B.J. Park, H.J. Choi, J.S. Choi, Thin Solid Films 518 (2009) 588.
[49] J. Park, S.D. Lee, B.J. Park, H.J. Choi, D.W. Kim, J.W. Lee, J.S. Choi, Mol. Cryst. Liq. Cryst. 51 (2010) 222.
[50] I.S. Lee, M.S. Cho, H.J. Choi, Polymer 46 (2005) 1317.
[51] T. Sawada, S. Ando, Chem. Mater. 10 (1998) 3368.
[52] R.K. Boggess, L.T. Taylor, J. Polym. Sci. Polym. Chem. Ed. 25 (1987) 685.
[53] J.D. Rancourt, L.T. Taylor, Macromolecules 20 (1987) 790.
[54] M.H. Tsai, C.J. Ko, Surf. Coat. Technol. 201 (2006) 4367.
[55] M. Stern, A.L. Geary, J. Electrochem. Soc. 104 (1957) 56.
[56] J. Bockris, K.N. Reddy, Modern Electrochemistry, John Wiley and Sons, New York, 1976.
[57] G. Grundmeier, W. Schmidt, M. Stratmann, Electrochim. Acta 45 (2000) 2515.
[58] Y. Zuo, R. Pang, W. Li, J.P. Xiong, Y.M. Tang, Corros. Sci. 50 (2008) 3322.
[59] S. Martinez, L.V. Žulj, F. Kapor, Corros. Sci. 51 (2009) 2253.
[60] S.M. Park, J.S. Yoo, Anal. Chem. A 75 (2003) 455.
[61] A. Amirudin, D. Thierry, Prog. Org. Coat. 26 (1995) 1.
[62] M.G. Medrano-Vaca, J.G. Gonzalez-Rodriguez, M.E. Nicho, M. Casales, V.M. Salinas-Bravo, Electrochim. Acta 53 (2008) 3500.
[63] S. Ray, K. Yamada, M. Okamoto, A. Ogami, K. Ueda, Chem. Mater. 15 (2003) 1456.
[64] H. Kawakami, K. Nakajima, H. Shimizu, S. Nagaoka, J. Membr. Sci. 212 (2003) 195.